# Unexpected Characteristics of the Isoscalar Monopole Resonances in the A ~ 90 region – Implications for Nuclear Incompressibility

Krishichayan[1,2],* D.H. Youngblood[2], Y.-W. Lui[2], J. Button[2], M.R. Anders[2], M.L. Gorelik[3], M.H. Urin[3], S. Shlomo[2]

[1]*Department of Pure & Applied Physics, Guru Ghasidas Central University, Bilaspur – 495009, INDIA*

[2]*Cyclotron Institute, Texas A&M University, College Station, TX 77843, USA*

[3]*National Research Nuclear University "MEPhI", Moscow, 115409, RUSSIA*

** email: krishichayan@gmail.com*

The isoscalar giant monopole resonances (ISGMR) in $^{90,92,94}$Zr and $^{92,96}$Mo have been studied with inelastic scattering of 240 MeV α particles at small angles including 0°. Strength corresponding to approximately 100% of the ISGMR (E0) energy-weighted sum rule was identified in each nucleus. In all cases the strength consisted of two components separated by 7-9 MeV. Except for the mass 92 nuclei, the upper component contained 14-22% of the E0 energy weighted sum rule (EWSR), however 38% and 65% of the E0 EWSR was located in the upper components in $^{92}$Zr and $^{92}$Mo respectively. The energies of the ISGMR for $^{92}$Zr and $^{92}$Mo are higher than for $^{90}$Zr, suggesting a significant nuclear structure contribution to the energy of the ISGMR in these nuclei. This has a large effect on the compression modulus of the nucleus.

## 1. Introduction

The giant resonances are small amplitude collective modes of excitations of nuclei and have been extensively studied since the discovery of the isovector giant dipole resonance (IVGDR) by Baldwin and Klaiber [1]. The study of the isoscalar giant monopole resonance (ISGMR), identified in 1977 [2], in which protons and neutrons in a nucleus move in-phase and oscillate with spherical symmetry, is important as it provides information about the incompressibility of finite nuclei, $K_A$, from which the incompressibility of infinite nuclear matter incompressibility, $K_{NM}$, can be obtained [3,4]. The incompressibility of finite nucleus is related to the GMR energy by

$$K_A = [M/\hbar^2]\langle r^2\rangle E_{GMR}^2 \qquad (1)$$

where in the scaling model $E_{GMR} = (m_3/m_1)^{1/2}$ and $m_k = \Sigma(E_n - E_0)k|\langle 0|r^2|n\rangle|^2$ is the kth moment of the strength distribution. There are, in general, two approaches to relate finite nucleus incompressibility, $K_A$, to the incompressibility of nuclear matter, $K_{NM}$. In the semi-empirical (macroscopic) approach, which is similar to the semi-empirical mass formula, $K_A$ is expressed as a Leptodermous ($A^{-1/3}$) expansion to parameterize $K_A$ into volume, surface, symmetry, and Coulomb terms [5,6]. $K_{NM}$ is identified with the volume term as

$$K_{NM} = \lim_{A\to\infty} K_A = K_{vol} \qquad (2)$$

(valid in scaling model only). In the microscopic approach, the strength function of the ISGMR is calculated using fully self consistent mean-field based random-phase approximation (RPA), with specific interactions [7] and compare with the experimental data. The values of $K_{NM}$ are then deduced from the interaction that best reproduced the experimental data. In 1999, measurements of the ISGMR for $^{40}$Ca, $^{90}$Zr, $^{116}$Sn, and $^{208}$Pb [8] were compared to HF-RPA calculations which used Gogny interaction [3] and took into account pairing and anharmonicity corrections, and a value for $K_{NM} = 231 \pm 5$ MeV was obtained. These data were of considerably higher quality than the data from the 70's and 80's (see Ref. [6] for detail). With the availability of a large amount of giant resonance data from 240-MeV α inelastic scattering using TAMU K500 cyclotron facility , Texas A&M group has studied the ISGMR in large number of nuclei in mass region $12 \le A \le 208$. In heavy nuclei ( $A \ge 110$) [9,10], the shape of ISGMR strength distribution is typically symmetric (with

Gaussian-like shape) whereas in light and medium-light mass nuclei the ISGMR strength is clearly broader and often split into more than one components [11-13] (see Fig. 1). As is seen in Fig. 1, in $^{208}$Pb, $^{144}$Sm, and $^{116}$Sn, ISGMR strength distribution is concentrated in what appears to be one symmetric peak (with Gaussian-like shape). In $^{60}$Ni, the ISGMR is asymmetric with a slower slope on the high excitation side of the peak whereas the structure of ISGMR is fragmented and complex in $^{48}$Ca. In $^{90}$Zr, the shape changes to mostly symmetric with a tail on the high excitation side of the ISGMR, as seen in Fig. 1. As we have seen from our data, the transition from mostly symmetric to asymmetric shape occurs at $^{90}$Zr region [14].

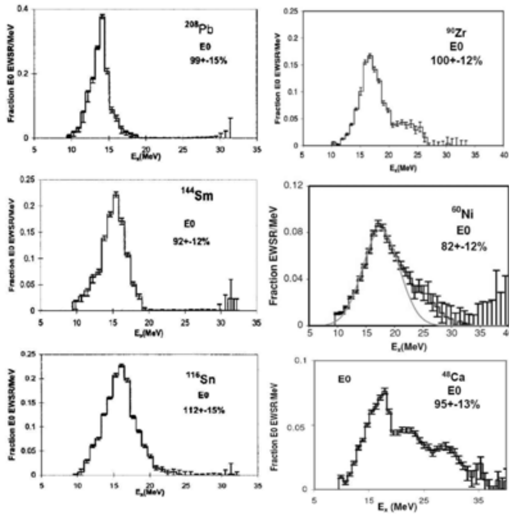


Fig.1 E0 strength distribution for nuclei in different mass region. Data taken from Refs. [9, 12-14].

In this article we report on measurements of the ISGMR in the A ~ 90 transition region, particularly, $^{90,92,94}$Zr and $^{92,96}$Mo where the GMR energies in the A=92 nuclei yield substantially higher nuclear compressibility than the other nuclei in this region (~27 MeV higher for $^{92}$Zr and ~56 MeV higher for $^{92}$Mo). These differences are not predicted with HF-RPA calculations that reproduce the ISGMR energies in the other isotopes and that are generally used to relate $K_{NM}$ to $K_A$. The origin of this discrepancy is unknown and raises the question of what is left out of such calculations, and how do these omissions affect $K_{NM}$.

## 2. Experimental technique

The experimental technique and detailed method of the analysis have been discussed thoroughly in Refs. [15-17] and are summarized briefly below. A beam of 240-MeV α particles from Texas A&M K500 superconducting cyclotron, after passing through a beam analysis system, bombarded self-supporting target foils (5-8 mg/cm$^2$ thick Zr and Mo foils each enriched to more than 96% in the desired isotope) located in the scattering chamber of the multipole-dipole-multipole (MDM) spectrometer. The horizontal acceptance of the spectrometer was 4$^o$ and the vertical acceptance was set at ±2$^o$. Ray tracing was used to reconstruct the scattering angle. Scattered particles entering the MDM spectrometer were momentum-analyzed and measured by a 60 cm long focal plane detector, which consisted of four resistive wire proportional counters to measure position, as well as an ionization chamber to provide ΔE and a plastic scintillator behind the ionization chamber to measure the energy deposited and provided a fast timing signal for each event. A position resolution of ~ 0.9 mm and scattering angle resolution of ~ 0.09$^o$ were obtained. The out–of-plane scattering angle was not measured. At $\theta_{spec}$ = 0$^o$, runs with an empty target frame had an α-particle rate approximately 1/2000th of that with a target in place, and α particles were uniformly distributed in the spectrum. The target thicknesses were measured by weighing and checked by measuring the energy loss of the 240-MeV α beam in each target. The data for each run were binned into ten angle bins by the horizontal angle. The scattering angle for each angle bin was obtained by integrating over the vertical opening of the slit. The differential cross section was extracted from the number of beam particles collected, the target thickness, the solid angle, the yields measured, and the dead time. The number of beam particles was monitored with a monitor detector at a fixed scattering angle in the scattering chamber. Dead time of the data taking system was measured by comparing the number of pulses sent to the system to those accepted. The cumulative uncertainties in the above parameters result in an approximately ±10% uncertainty in absolute cross sections. $^{24}$Mg spectra were taken before and after each run, and the 13.85 ± 0.02 MeV L = 0 state [18] was used as a check on the calibration in the giant resonance region. Initially data were taken for $^{90,92}$Zr and $^{92}$Mo and analysis revealed the behaviour in the A = 92 nuclei reported here. In an additional experimental run, data were taken for $^{92}$Mo, $^{94}$Zr, and $^{96}$Mo. The $^{92}$Mo strength distributions obtained in the two experiments are in excellent agreement.

Sample spectra obtained are shown on Fig. 2. The spectrum was divided into a peak and a continuum where the continuum was assumed to have the shape of a straight line at high excitation joining onto a Fermi shape at low excitation to model particle threshold effects [19]. Samples of the continua used are also shown in Fig. 2. The giant resonance peak can be seen extending up to $E_x \sim 35$ MeV.

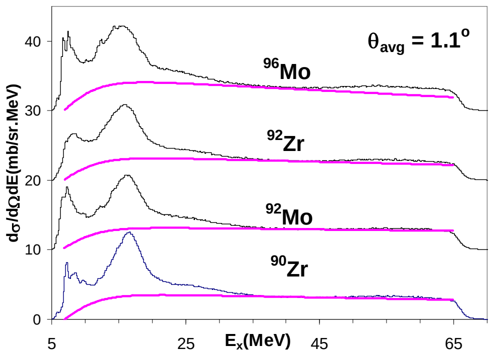


**Fig. 2** Inelastic α spectra obtained with the spectrometer at 0° for $^{90}$Zr, $^{92}$Mo (offset 10 units), $^{92}$Zr (offset 20 units) and $^{96}$Mo (offset 30 units). The thick lines show continua chosen for the analysis.

## 3. Data analysis and results

The mulitpole components of the giant resonance peak were obtained [15-17] by dividing the peak into multiple regions (bins) by excitation energy and then comparing the angular distributions obtained for each of these bins to distorted wave Born approximation (DWBA) calculations. The uncertainty from the multipole fits was determined for each multipole by incrementing (or decrementing) that strength, then adjusting the strengths of the multipoles to minimize total $\chi^2$. This continued until the new $\chi^2$ was one unit larger than the total $\chi^2$ obtained for the best fit. Optical parameters for the calculations were determined from elastic scattering for $^{90}$Zr [20] and are given in Table 1 along with Fermi parameters used for the density distribution of the nuclear ground state.

Table 1: Optical and Fermi parameters used in DWBA calculations

| V (MeV) | $W_i$ (MeV) | $r_i$ (fm) | $a_i$ (fm) | c (fm) | a (fm) |
|---|---|---|---|---|---|
| 40.2 | 40.9 | 0.786 | 1.242 | 4.901 | 0.515 |

The DWBA calculations were performed, as prescribed in Refs. [21, 22], using the density-dependent single-folding model for the real part, obtained with a Gaussian α-nucleon potential, and a phenomenological Woods-Saxon potential for the imaginary term. The α-nucleus interaction is given by given by

$$U(r)=VF(r)+iW/\{1+\exp[(r-R_i)/a_i]\}, \quad (3)$$

where VF(r) is the real single-folding potential obtained by folding the ground-state density with the density-dependent α-nucleon interaction,

$$vDDG(s,\rho) = -v[1- \alpha\rho(r')\beta] \exp[-s^2/t^2], \quad (4)$$

where s = |r-r’| is the distance between the center of mass of the alpha particle and a target nucleon, $\rho(r') = \rho_0(1+e[(r'-c)/a])-1$ is the ground-state density of the target nucleus at the position r’ of the target nucleon, $\alpha = 1.9$ fm$^2$, $\beta = 2/3$, and t (range) = 1.88 fm. W, $R_i$, and $a_i$ are WS parameters for the imaginary potential. These calculations were carried out with the code PTOLEMY [23]. Since PTOLEMY calculates all kinematics non-relativistically, corrections to the projectile mass and lab energy were made to achieve a proper relativistic calculation [24]. The shape of the real part of the potential and the form factor for PTOLEMY were obtained using the codes SDOLFIN and DOLFIN [25]. The transition densities and sum rules for various multipolarities are discussed thoroughly in Ref. [15] and, except for the ISGDR, the same expressions and techniques were used in this work. The transition density for inelastic alpha-particle excitation of the ISGDR given by Harakeh and Dieperink [26] (and described in Ref. [15]) is for only one magnetic substate, so that the transition density given in Ref. [15] must be multiplied by √3 in the DWBA calculations. The isoscalar E0 multipole distributions obtained for Zr and Mo isotopes are shown in Fig. 3. Several analyses were carried out to access the effects of different choices of the continuum on the multipole distributions as described in Ref. [19]. The errors shown on the strength distributions were calculated by adding the errors obtained from the multipole fits in quadrature to the standard deviations between the different analyses. Energies and sum rule strengths obtained are summarized in Table 2. E0 strength identified in each nucleus corresponded within errors to 100% of the E0 EWSR. The results obtained for $^{90}$Zr are in excellent agreement with our previous results [8,19]. While $E_{GMR}$

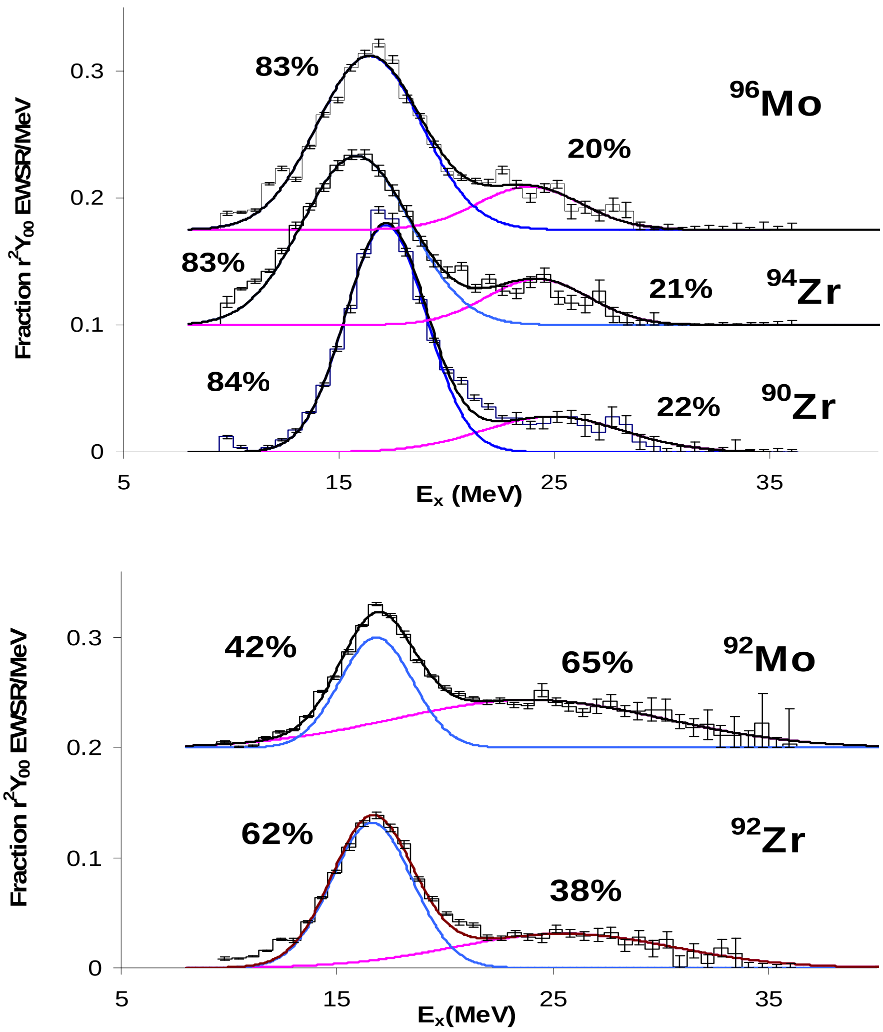


**Fig.3** The black histograms show the fraction of the $r^2Y_{00}$ sum rule obtained for Mo and Zr isotopes plotted as a function of excitation energy. Superimposed are Gaussian fits to the two components of the distributions as well as the sum of the fits. On the left side are the strengths of the lower energy peak while on the right side the strengths of the higher energy peaks are listed, all given as a percentage of the $r^2Y_{00}$ sum rule.

generally decreases as *A* increases (this is small in adjacent nuclei), $E_{GMR}$ for $^{92}$Zr and $^{92}$Mo are 1.22 MeV and 2.80 MeV, respectively, higher than for $^{90}$Zr, a surprising result. In all of these nuclei, the E0 strength consists of a relatively narrow peak, with significant tailing at higher excitation. In order to provide a consistent framework to compare the results for the different nuclei, the E0 distributions were fit with two Gaussians. For the nuclei with A ≠ 92, 80-90% of the strength is in the lower energy peak located at 15.7 to 17.2 MeV, with the remaining 10 to 20% located in a broad peak centered at $E_x$ ~ 25 MeV. It is clear that the distribution of the E0 strength in $^{92}$Mo is dramatically different from the others, with only 40% of the observed strength in the lower peak and 60% in the upper peak. In $^{92}$Zr, the lower peak contains 65% and the upper peak 35% of the observed E0 strength. While the overall E0 strength could be affected somewhat by raising or lowering the assumed continuum, the dramatic difference in strength distributions between $^{90}$Zr and $^{92}$Mo could be reduced significantly only by assuming that the shape and strength of the continuum changes radically relative to the strength above the resonance region as a function of angle, and changes very differently for different nuclei. The isoscalar giant quadrupole resonance(GQR) is located just below the ISGMR and the GQR strength extracted for all the nuclei is concentrated in symmetrical peaks containing 80~ 95% of the E2 EWSR. In $^{90}$Zr, $^{92}$Zr, and $^{92}$Mo, $E_{GQR}$ = 14.30±0.15, 14.02±0.15 and 14.53±0.15 MeV respectively, having RMS widths of 4.8, 5.5 and 6.3 MeV. There is no tailing of the quadrupole strength in any of the nuclei studied and $E_{GQR}$ for the mass 92 nuclei are within errors the same as $^{90}$Zr. Prior to our 240 MeV α work reported in 1999 [8], the strength in $^{90}$Zr at ~ 23-25 MeV had not been seen due in part to the much higher continuum/background present in the earlier (lower energy) studies [27,28] and in part to the assumption that any strength above the unresolved GQR-ISGMR peak was part of the continuum/background. In these earlier works it was also assumed that the strength in each giant resonance was concentrated in a single Gaussian peak.

Table 2. Parameters obtained for the E0 (in % EWSR) distributions shown in Fig. 3. Uncertainties include systematic errors. $E_{GMR}$ is given by the ratio of energy moments $(m_3/m_1)^{1/2}$ for the scaling model**.**

| | | | | Gaussian Peak | | | | | |
|---|---|---|---|---|---|---|---|---|---|
| | | $E_{GMR}$ | Centroid | Low Peak | | | High Peak | | |
| Nucleus | % E0 | $(m_3/m_1)^{1/2}$ (MeV) | $m_1/m_0$ (MeV) | $E_x$ MeV | Γ MeV | % E0 | $E_x$ MeV | Γ MeV | % E0 |
| $^{90}$Zr | 106±12 | 18.86+.23-.14 | 17.88+.13-.11 | 17.1 | 4.4 | 84 | 24.9 | 7.6 | 22 |
| $^{92}$Zr | 103±12 | 20.09+.31-.22 | 18.23+.15-.13 | 16.6 | 4.4 | 62 | 25.5 | 12.0 | 38 |
| $^{94}$Zr | 106±12 | 17.52+.18-.14 | 16.16+.12-.11 | 15.8 | 5.9 | 83 | 24.2 | 5.6 | 21 |
| $^{92}$Mo | 107±13 | 21.68+.53-.33 | 19.62+.28-.19 | 16.8 | 4 | 42 | 23.9 | 14.7 | 65 |
| $^{96}$Mo | 105±12 | 18.18+.20-.13 | 16.95+.12-.10 | 16.4 | 5.7 | 83 | 23.8 | 5.7 | 20 |

A study of $^{90}$Zr at Osaka with 400 MeV α particles [29] showed the E0 strength with a peak at $E_x$ = 16.6 MeV and continuous E0 strength through 32 MeV, the highest energy reported, which would mask the strength we see. Most of the multipole distributions in most of the nuclei reported by the Osaka group [29,30] show continuous strength above the giant resonance peak to the highest energy studied, and they argue that this continuous strength must be spurious. In most cases, if this strength were real, they would identify significantly more than 100% of the EWSR for each multipole.

The ISGMR's in $^{92}$Mo and $^{96}$Mo were studied with $^3$He inelastic scattering [27] in 1983 where they located 24% and 19% of the E0 EWSR respectively, in Gaussian peaks at $E_x$ =16.35 MeV and 16.40 MeV, respectively. The same group later used 152 MeV α inelastic scattering [31] to study $^{92}$Mo where they reported 84% ± 17% of the strength in a peak at $E_x$ = 16.2 MeV with a width Γ= 4.8 MeV. Though both $^3$He and α result are listed in the table in Ref. [31], the authors do not comment on the reason for the discrepancy between them. In both these works, the authors assumed that the E0 strength was located in a single Gaussian peak and all cross section at energies above $E_x$ ~ 21 MeV was attributed to the continuum/background. We now know that giant resonance strength extends up to $E_x$ ~ 35 MeV in most nuclei [8,9,13,19]. Their continuum/background assumptions precluded identification of any strength above $E_x$ ~21 MeV. The calculations used to normalize the strength were carried out with the deformed potential model, and it has been shown [32] that reliable strengths can be obtained only with folding calculations, so that the uncertainties would be larger if the uncertainties in the calculations were included.

Within the scaling model [33], the ISGMR energy is given by $E_{GMR} =(m_3/m_1)^{1/2}$,where $m_k$ is the k-th energy moment of the strength distribution. Using for $E_{GMR}$ the experimental energies corresponding to the scaling model $\{(m_3/m_1)^{1/2}\}$ shown in Table 1 and radii obtained from Hartree-Fock calculations [34] with the KDE0v1 interaction [35] having $K_{NM}$ = 227.5 MeV, the experimental scaling model values of $K_A$ for the Zr and Mo isotopes were obtained from Eq. (1). For $^{92}$Zr and $^{92}$Mo, $K_A$ values obtained from the experimental energies are 27 MeV and 56 MeV higher than the values predicted with HF-RPA.

To attempt to understand this behavior, we calculated microscopic transition densities for $^{92}$Mo using Woods-Saxon based RPA and used them to calculate cross sections for E0 excitation at $E_x$ =17.5 MeV and 27.5 MeV. Using the collective transition density, the cross section for excitation of the ISGMR at Ex =27.5 MeV is ~1/5 that at Ex = 17.5 MeV, whereas with the microscopic transition density this ratio is ~ 1/12. Thus, using the microscopic transition density will enhance the upper peak by more than a factor of 2 in $^{92}$Mo and result in the upper peak alone exhausting more than 100% of the EWSR and shifting $E_{GMR}$ to even higher energy, further increasing $K_A$ for $^{92}$Mo.

We also investigated the possibility that this second peak could be the "overtone" ISGMR (operator $r^4Y_{00}$) [37]. Using the collective transition density and sum rule for the overtone, two calculations were done for $^{92}$Mo (the results based on these calculations are preliminary). The first assumed that the second peak was entirely due to the overtone. That would require 228% of the sum rule for the overtone and leave only the 42% of the $r^2Y_{00}$ in the lower peak (lower panel Fig. 4). We then placed the overtone at twice the energy of the ISGMR with twice the width, with 100% of the $r^4Y_{00}$ sum rule and subtracted that from the $^{92}$Mo E0 strength. This is shown in the upper panel of Fig. 4 and leaves E0 strength corresponding to 91% of the $r^2Y_{00}$ sum rule, which is quite plausible. Unfortunately this interpretation does not work for $^{90}$Zr or $^{96}$Mo, because the $r^4Y_{00}$ strength would considerably exceed the strength seen experimentally in the higher energy region. $E_{GMR}$ for the calculation in the bottom panel is 20.15 MeV, resulting in $K_A$ of 179 MeV, 27 MeV above that expected from the HF-RPA calculations. While this reduces the discrepancy for $^{92}$Mo (and could eliminate it for $^{92}$Zr), there is no obvious reason for the overtone to be present in A=92 nuclei, and absent for the other nuclei.

Thus we are left with the conclusion that the E0 strength distributions observed are due to the ISGMR and those in the A = 92 nuclei lead to much higher nuclear compressibilities (particularly for $^{92}$Mo) than the other nuclei in this region, which raises serious questions about the influence of nuclear structure on the energy of the ISGMR and hence about nuclear matter compressibility extracted from these energies. The ISGMR energy is significantly affected by the properties of the individual nucleus in a manner not accounted for in HF-based RPA calculations that relate ISGMR energies to KNM and hence is not a good indicator of compressibility in these A = 92 nuclei.

We have also taken data for $^{98,100}$Mo to further explore this behaviour in mass 90 region and the data is being analyzed.

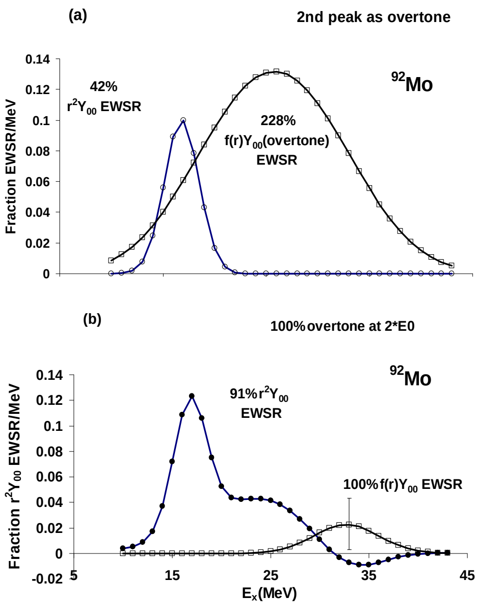


**Fig. 4** (Preliminary results) (a) ISGMR strength distributions for $^{92}$Mo obtained by assuming that the lower peak (diamonds) is due entirely to ISGMR excitation and the upper peak (squares) is due entirely to overtone excitation are plotted versus excitation energy. The percentages of the respective sum rules are indicated. The vertical scale for the lower peak is relative to the $r^2Y_{00}$ sum rule, while that for the upper peak is relative to the $f(r)Y_{00}$ sum rule.

(b) The strength distribution obtained for the overtone in $^{92}$Mo located at twice the energy of the lower peak with twice the width and containing 100% of the $f(r)Y_{00}$ sum rule is shown by the squares plotted versus excitation energy. The diamonds show the strength remaining after this is subtracted from the strength shown in Fig. 3. The vertical scale is relative to the $r^2Y_{00}$ sum rule. The error bar indicates the experimental error at $E_x$ = 33 MeV.

## Acknowledgments

This work was supported in part by the U.S. Department of Energy under grant DE-FG03-93ER40773.

## References

[1] G.C. Baldwin, and G.S. Klaiber, Phys. Rev. 71, 3 (1947).
[2] D.H. Youngblood, C.M. Rozsa, J.M. Moss, D.R. Brown, and J.D. Bronson, Phys. Rev. Lett. 39, 1188 (1977).
[3] J.P. Blaizot, J.F. Berger, J. Decharge, M. Girod, Nucl. Phys. A 591, 435 (1995).
[4] J.P. Blaizot, Phys. Rep. 64, 171 (1980).
[5] J. Treiner, H. Krivine, and O. Bohigas, Nucl. Phys. A371, 253 (1981).
[6] S. Shlomo and D.H. Youngblood, Phys. Rev. C 47, 529 (1993), and references therein.
[7] S. Shlomo, V. M. Kolomietz, and G. Colo, Eur. Phys. J. A30, 23 (2006) and references therein.
[8] D.H. Youngblood, H.L. Clark, and Y.-W. Lui, Phys. Rev. Lett. 82, 691 (1999).
[9] D.H. Youngblood, Y.-W. Lui, H.L. Clark, B. John, Y. Tokimoto, and X. Chen, Phys. Rev. C69, 034315 (2004).
[10] Y.-W. Lui, D.H. Youngblood, H.L. Clark, and B. John, Phys. Rev. C 69, 034611 (2004).
[11] D.H. Youngblood, Y.-W. Lui, Y. Tokimoto, H.L. Clark, B. John, Phys. Rev. C68, 057303 (2003); D.H. Youngblood, Y.-W. Lui, H.L. Clark, Phys. Rev. C63, 067301 (2001).
[12] Y.-W. Lui, D.H. Youngblood, H.L. Clark, Y. Tokimoto, and B. John, Phys. Rev. C73, 014314 (2006).
[13] Y.-W. Lui, D.H. Youngblood, S. Shlomo, X. Chen, Y. Tokimoto, Krihsichayan, M. Anders, and J. Button, Phys. Rev. C83, 044327 (2011).
[14] D.H. Youngblood, Y.-W. Lui, B. John, Y. Tokimoto, H.L. Clark, and X. Chen, Phys. Rev. C69, 054312 (2004).
[15] D.H. Youngblood, Y.-W. Lui, and H.L. Clark, Phys. Rev. C 55, 2811 (1997).
[16] D.H. Youngblood, Y.-W. Lui, and H.L. Clark, Phys. Rev. C 60, 014304 (1999).
[17] D.H. Youngblood, Y.-W. Lui, and H.L. Clark, Phys. Rev. C 65, 034302 (2002).
[18] K. van der Borg, M.N. Harakeh, and A. van der Wounde, Nucl. Phys. A 365, 243 (1981).

[19] D.H. Youngblood, Y.-W. Lui, B. John, Y. Tokimoto, H.L. Clark, and X. Chen, Phys. Rev. C 69, 054312 (2004).
[20] H.L. Clark, Y.-W. Lui, and D.H. Youngblood, Nucl. Phys. A687, 80c (2001).
[21] G.R. Satchler and D.T. Khoa, Phys. Rev. C 55, 285 (1997).
[22] H.L. Clark, Y.-W. Lui, and D.H. Youngblood, Phys. Rev. C 57, 2887 (1998).
[23] M. Rhoades-Brown, M.H. Macfarlane, and S.C. Pieper, Phys. Rev. C 21, 2417 (1980); M.H. Macfarlane and S.C. Pieper, Argonne National Laboratory Report No. ANL-76-11, 1978 (unplished).
[24] G.R. Satchler, Nucl. Phys. A 540, 533 (1992).
[25] L.D. Rickerston, The folding program DOLFIN, 1976 (unpublished).
[26] M.N. Harakeh and A.E.L. diepernik, Phys. Rev. C 23, 2329 (1981)
[27] M. Buenerd, in Proceedings of International Symposium on Highly Excited States and Nuclear Structure, Orsay, France, edited by N. Marty and N. Van Giai, J. Phys. (Paris) Colloq. 45, C4-115 (1984).
[28] D.H. Youngblood, P. Bogucki, J.D. Bronson, U. Garg, Y.-W. Lui, and C.M. Rozsa, Phys. Rev. C 23, 1997 (1981).
[29] M. Uchida et al., Phys. Rev. C 69, 051301(R)(2004).
[30] T. Li et al. Phys. Rev. Lett. 99, 162503 (2007); T. Li et al. Phys.Rev.C 81, 034309 (2010).
[31] G. Duhamel, M. Buenerd, P. de Saintignon, J. Chauvin, D. Lebrun, Ph. Martin and G. Perrin, Phys. Rev. C 38, 2509 (1988).
[32] J.R.Beene, D.J. Horen, and G.R. Satchler, Phys. Lett. B344, 67 (1995).
[33] J. Treiner, H. Krivine and O. Bohigas, Nucl. Phys. A371, 253 (1981).
[34] M.R. Anders (private communication).
[35] B.K. Agrawal, S. Shlomo and V. Kim Au, Phys. Rev. C 72, 014310(2005).
[36] M.L. Gorelik, I.V. Safonov and M.H. Urin, Phys. Rev. C 69, 054322 (2004).
[37] S. Shlomo, V.M. Kolomietz and B.K. Agrawal, Phys. Rev. C 68, 064301 (2003).
[38] D.H. Youngblood, Y.-W. Lui, H.L. Clark, B. John, Y. Tokimoto, and X. Chen, Phys. Rev. C 69, 034315 (2004).
[39] Y.–W. Lui, D.H. Youngblood, Y. Tokimoto, H.L. Clark, and B. John, Phys. Rev. C 70, 014307(2004).
[40] J. Piekarewicz, Phys. Rev. C 76, 031301(R)(2007).
[41] U. Garg et al., Nucl. Phys. A788, 36c (2007).